Catalysis Science & Technology

ROYAL SOCIETY OF CHEMISTRY

PAPER

View Article Online
View Journal

Cite this: DOI: 10.1039/d6cy00522e

Acidity regulation of Ni–Fe/ZSM-5 catalysts for enhanced lipid deoxygenation toward renewable diesel production

Qing Li,†[b] Zihao Gao,†[a] Fumin Wang,[a] Fei Wang,*[b] Junfeng Feng,[c] Yuwei Chen,[d] Baining Lin,*[e] Xudong Liu,[e] Rukuan Liu*[e] and Dechao Wang*[f]

Received 21st April 2026,
Accepted 17th May 2026

DOI: 10.1039/d6cy00522e

rsc.li/catalysis

Catalytic deoxygenation of lipids provides a promising route for producing renewable diesel-range hydrocarbons. Herein, a series of Ni–Fe/ZSM-5 catalysts with different Si/Al ratios were prepared to clarify the correlation between catalyst acidity and lipid deoxygenation performance. Comprehensive characterization confirmed that adjusting the Si/Al ratio could precisely regulate the acidity, metal dispersion and textural properties of the catalysts, which significantly governed catalytic activity and product selectivity. Notably, the Ni–Fe/ZSM-5 catalyst with a Si/Al ratio of 25 achieved the best activity and maximum selectivity toward diesel-range alkanes. The appropriate acid site density and highly dispersed Ni–Fe bimetallic sites facilitated the hydrodeoxygenation (HDO) pathway and simultaneously inhibited undesired cracking reactions. Additionally, the Ni–Fe synergistic effect effectively improved catalytic stability. This work demonstrates that acidity regulation of ZSM-5-supported non-noble metal catalysts is an effective strategy for enhancing lipid deoxygenation toward renewable diesel production.

1. Introduction

The increasing consumption of fossil fuels has triggered severe environmental pollution and mounting global concerns over energy security. Consequently, the development of sustainable and renewable energy sources has become a pivotal research focus worldwide.[1–3] Among diverse renewable resources, biomass-derived fuels have attracted extensive attention due to their abundant reserves, carbon-neutral characteristics, and great potential to partially replace petroleum-based fuels. Lipids, including used cooking oil (UCO), palm oil mill effluent (POME), inedible vegetable oils, and microalgae oils, represent highly promising feedstocks for the production of bio-based liquid fuels, owing to their high energy density and widespread availability.[4,5] Conventionally, lipids are converted into biodiesel *via* transesterification to produce fatty acid methyl esters (FAMEs).[6,7] Despite the wide commercialization of this first-generation biodiesel technology, the obtained FAME fuels suffer from high oxygen content, unsatisfactory oxidative stability, and poor low-temperature properties. As a result, FAMEs usually need to be blended with fossil diesel before use in conventional diesel engines.[8,9] In contrast, the catalytic deoxygenation of lipids offers a competitive alternative route to produce second-generation biodiesel, also referred to as renewable diesel or green diesel. Through deoxygenation reactions, triglycerides and fatty acids can be converted into hydrocarbons with chemical compositions similar to those of petroleum-derived diesel fuels. These hydrocarbons deliver excellent fuel properties and can be directly used in existing diesel engines without further modification.[10–12]

During lipid deoxygenation, triglycerides are initially converted into free fatty acids *via* thermal decomposition or hydrolysis. The resulting fatty acids then proceed through three distinct primary reaction pathways: hydrodeoxygenation (HDO), decarboxylation (DCX), and decarbonylation (DCN).[13] In the HDO pathway, oxygen is removed in the form of water, producing hydrocarbons retaining the full carbon chain length of the parent fatty acids. In contrast, the DCX and DCN pathways generate hydrocarbons with one fewer carbon atom, accompanied by the release of CO_2 or CO.[14] From an

[a] School of Chemical Engineering and Technology, Tianjin University, Tianjin 300072, China
[b] School of Energy & Mechanical Engineering, Nanjing Normal University, Nanjing 210023, China. E-mail: feiwang@njnu.edu.cn
[c] College of Chemical Engineering, Jiangsu Co-Innovation Centre of Efficient Processing and Utilization of Forest Resources, Jiangsu Provincial Key Lab for the Chemistry and Utilization of Agro-forest Biomass, Nanjing Forestry University, Nanjing 210037, China
[d] School of Automotive Engineering, Yancheng Institute of Technology, Yancheng 224051, China
[e] State Key Laboratory of Woody Oil Resource Utilization, Hunan Academy of Forestry, Changsha 410018, China. E-mail: baininglin1995@163.com, liurukuan@hnlky.cn
[f] College of Energy, Xiamen University, Xiamen 361102, Fujian, China. E-mail: wangdechao@xmu.edu.cn
† Q. Li and Z. Gao contributed equally.

industrial perspective, the HDO route is exclusively preferred because it minimizes carbon loss and maximizes hydrocarbon yield, which is critical for process economics. Catalysts play a decisive role in governing the activity, product selectivity, and dominant reaction pathway of lipid deoxygenation. Noble metal catalysts and sulfided molybdenum-based catalysts have been widely investigated for this process due to their excellent hydrogenation activity. However, the prohibitive cost of noble metals and the mandatory requirement for continuous sulfur addition to maintain activity in molybdenum-based systems severely hinder their large-scale industrial deployment.[15–17] In recent years, transition-metal-based catalysts, particularly Ni-based catalysts, have emerged as promising alternatives owing to their relatively low cost and favorable hydrogenation activity. As demonstrated in our previous studies, the incorporation of a second metal (*e.g.*, Fe) can effectively mitigate coke formation, enhance metal dispersion, and simultaneously improve catalytic activity and long-term stability.[10,18,19]

For Ni-based catalysts, various metal oxides and carbonaceous supports (*e.g.* Al_2O_3, SiO_2, ZrO_2, and activated carbon) have been widely used. However, lipid deoxygenation over these conventional catalysts typically proceeds predominantly *via* the DCX/DCN pathways rather than the desired HDO, resulting in substantial carbon loss and reduced hydrocarbon yields. Previous studies have shown that introducing acidic sites into the catalyst system can regulate the reaction pathway by facilitating the dehydration of intermediate fatty alcohols, which are subsequently hydrogenated to alkanes, thereby shifting the reaction selectivity toward the HDO pathway. ZSM-5 zeolite is a versatile catalytic material owing to its unique MFI microporous structure, excellent hydrothermal stability, tunable Brønsted acidity, and readily constructible hierarchical pore structure.[20,21] Notably, the acidity of ZSM-5 can be precisely tailored by adjusting the Si/Al molar ratio, as the framework aluminum content directly determines the density and distribution of Brønsted acid sites. Therefore, precise control of the Si/Al ratio provides an effective strategy to regulate catalyst acidity and potentially optimize the reaction pathway for lipid deoxygenation.[22] Despite these compelling advantages, studies on ZSM-5-supported Ni-based catalysts for lipid deoxygenation remain relatively limited. In particular, the quantitative relationship between catalyst acidity, tuned by the Si/Al ratio, and catalytic activity, product selectivity, and reaction pathway distribution has not been systematically elucidated. Furthermore, the trade-off between HDO promotion and excessive cracking induced by acid sites remains poorly understood.

Herein, a series of ZSM-5 zeolites with systematically varied Si/Al molar ratios (15–110) were hydrothermally synthesized to regulate catalyst acidity. Bimetallic Ni–Fe catalysts supported on these ZSM-5 materials were prepared *via* a facile impregnation method and evaluated for selective lipid deoxygenation to diesel-range hydrocarbons. Comprehensive characterization was performed to reveal the intrinsic correlations between catalyst structure, acidity, metal dispersion, and catalytic performance. Additionally, the effects of reaction temperature and diverse lipid feedstocks (including fatty acid substrates, soybean oil, microalgae oil, used cooking oil, and palm oil mill effluent) on deoxygenation performance were systematically investigated. The findings provide fundamental insights into the rational design of high-performance catalysts for the sustainable conversion of lipid biomass into renewable diesel.

2. Experimental

2.1 Chemicals

All chemicals were purchased and used directly without purification. Sodium aluminate ($NaAlO_2$ >99%, as the aluminum source), tetraethyl orthosilicate (TEOS, 98%), sodium hydroxide (NaOH, 96%), tetrapropylammonium hydroxide (TPAOH, 25% solution in methanol), ammonium chloride (NH_4Cl, 99%), nickel nitrate hexahydrate ($Ni(NO_3)_2{\cdot}6H_2O$, AR), ferric nitrate nonahydrate ($Fe(NO_3)_3{\cdot}9H_2O$, AR), and fatty acid substrate (FA) were purchased from Shanghai Macklin Biochemical Technology Co., Ltd. The soybean oil and microalgae oil were bought from a local supermarket and Xiamen Blue Biological Technology Co., Ltd. (China), respectively. The pretreated UCO and POME were provided from Hainan Huanyu New Energy Co., Ltd. The model fatty acid (FA) feedstock consisted predominantly of oleic acid (C18:1, 96.9 wt%), with a small fraction of palmitoleic acid (C16:1, 3.1 wt%). The fatty acid compositions of the lipid-derived feedstocks were also determined. Soybean oil contained 92.7 wt% C18:1 and 7.3 wt% C16:1. Used cooking oil (UCO) was composed of 39.0 wt% C18:1 and 61.0 wt% C16:1, while palm oil mill effluent (POME)-derived lipids contained 54.0 wt% C18:1 and 46.0 wt% C16:1. Microalgae oil showed a broader fatty acid distribution, mainly including C22:2 (51.6 wt%), C16:1 (43.2 wt%), C20:0 (2.9 wt%), and C18:1 (2.3 wt%).

2.2 Ni–Fe/ZSM-5 catalyst preparation

2.2.1 Synthesis of ZSM-5 carriers. A series of ZSM-5-*x* supports (where *x* denotes the nominal Si/Al molar ratio) were synthesized *via* a facile hydrothermal method.[23–25] The molar ratio of SiO_2 to Al_2O_3 was precisely adjusted by varying the dosages of $NaAlO_2$ and TEOS to obtain target Si/Al ratios of 15, 25, 45, 65, 85, and 110. Taking the synthesis of ZSM-5-25 as a representative example: initially, 0.15 g of $NaAlO_2$ and 0.15 g of NaOH were dissolved in 4.9 g of deionized water. Subsequently, 9.5 g of TPAOH was added as a structure-directing agent, and the mixture was stirred for 1 h. Finally, 9.8 g of TEOS was dropped dropwise slowly, followed by vigorous stirring for an additional 2 h to form a homogeneous gel with a molar composition of 1 Al_2O_3 : 100 SiO_2 : 20 TPA_2O–4 Na_2O–200 H_2O. The resulting gel was transferred to a 100 mL Teflon-lined stainless-steel autoclave, aged at 80 °C for 5 h, and then crystallized at 170 °C for 24 h. The white solid was collected by filtration, washed repeatedly

with deionized water until the filtrate reached neutral pH, dried in an oven at 105 °C for 12 h, and calcined in a muffle furnace at 550 °C for 6 h with a heating ramp of 10 °C min^{-1} under an air atmosphere to obtain Na-type ZSM-5 (Na-ZSM-5). To convert Na-ZSM-5 to proton-type ZSM-5 (H-ZSM-5), the as-synthesized Na-ZSM-5 was subjected to three consecutive ion-exchange cycles in 0.8 mol L^{-1} NH_4Cl aqueous solution at 80 °C for 6 h each, followed by calcination at 550 °C for 6 h under the same conditions.

2.2.2 Synthesis of Ni–Fe/ZSM-5-*x* catalysts. Bimetallic Ni–Fe/ZSM-5-*x* catalysts were synthesized *via* a conventional wet impregnation method. Initially, 2.0 g of the as-synthesized H-ZSM-5-*x* support, stoichiometric amounts of $Ni(NO_3)_2{\cdot}6H_2O$ and $Fe(NO_3)_3{\cdot}9H_2O$ (at a fixed Ni/Fe molar ratio), and 12.0 g of deionized water were mixed and magnetically stirred for 3 h at room temperature to form a uniform suspension. Excess water was subsequently removed under reduced pressure using a rotary evaporator. The obtained solid was dried in an oven at 105 °C for 12 h, and then calcined in a muffle furnace at 550 °C for 3 h with a heating ramp of 10 °C min^{-1} under a static air atmosphere. Prior to catalytic testing, the calcined precursors were reduced in a tubular furnace at 400 °C for 3 h under a 10% H_2/Ar flow (50 mL min^{-1}) to obtain metallic active sites. To prevent spontaneous oxidation of the highly reactive reduced metal species upon exposure to ambient air, the catalysts were passivated *in situ* at room temperature for 3 h under a flow of 1% O_2 balanced with 99% N_2. A series of Ni–Fe/ZSM-5-*x* catalysts with Si/Al ratios of 15, 25, 45, 65, 85, and 110 were prepared following this identical procedure.

2.3 Catalyst characterization

X-ray diffraction (XRD) spectra were recorded on a D-POWER X-ray diffractometer (GKINST Co., Ltd.) to identify the crystalline phases of the catalysts. The instrument was operated at 40 kV using Cu Kα radiation (λ = 0.15406 nm). The diffraction data were collected in the 2θ range from 5.0 to 90.0° with a scanning rate of 10° min^{-1}. The average crystallite size of metallic Ni was calculated using the Scherrer equation based on the characteristic diffraction peak of Ni(111) at 44.5°. Nitrogen physisorption measurements were performed on a QUANTA N_2 adsorption–desorption analyzer (USA) at −196 °C to determine the specific surface area and pore structure parameters of the catalysts. Prior to measurement, all samples were degassed under vacuum at 200 °C for 10 h to remove physically adsorbed water and impurities. X-ray photoelectron spectroscopy (XPS) was conducted on a Thermo Scientific ESCALAB Xi+ using an Al Kα X-ray source. All binding energies were calibrated against the adventitious C 1s peak at 284.8 eV to eliminate charging effects. The XPS spectra were fitted using Avantage software. Temperature-programmed desorption of ammonia (NH_3-TPD) was conducted on a Micromeritics AutoChem II 2920 instrument to characterize the acid properties of the catalysts. Typically, 0.1 g of the calcined catalyst was accurately weighed and loaded into a quartz tube. The sample was first reduced in a 10% H_2/90% Ar gas stream (50 mL min^{-1}) at 400 °C for 3 h with a heating rate of 10 °C min^{-1}, then purged with pure Ar (100 mL min^{-1}) at 450 °C for 30 min to remove adsorbed species. After cooling to 50 °C, the sample was exposed to a 4% NH_3/He gas stream (50 mL min^{-1}) for 1 h to saturate the acid sites. Subsequently, physically adsorbed NH_3 was removed by purging with pure He (100 mL min^{-1}) at 50 °C for 1 h. Finally, the temperature was raised from 50 to 800 °C at a heating rate of 10 °C min^{-1}, and the desorbed NH_3 was detected using a thermal conductivity detector (TCD).

2.4 Lipid deoxygenation and product analysis

Catalytic deoxygenation of lipids was carried out in a 100 mL batch reactor (YZRJ-100, Shanghai Yanzheng Experimental Instruments Co., Ltd, China). The reaction procedure was based on our previous studies.[14,26] Typically, 0.25 g of the as-prepared passivated Ni–Fe/ZSM-5-*x* catalyst, 2.0 g of lipid substrates (FA, UCO, POME, microalgae oil, and soybean oil), and 20.0 g of *n*-dodecane (as the solvent) were added into the reactor. The mixture was magnetically stirred at 500 rpm throughout the reaction. Prior to heating, the reactor was purged with high-purity H_2 3 times to completely remove residual air. The reactor was then pressurized with H_2 to 2.0 MPa, heated to the target temperature at a rate of 5 °C min^{-1}, and maintained for 3 h. After the reaction, the reactor was rapidly cooled to room temperature in an ice-water bath to terminate the reaction. The liquid product was collected by filtration through a 0.22 μm organic filter membrane. All deoxygenation experiments were repeated at least three times to ensure the reliability and reproducibility of the experimental data.

The stability and reusability of the Ni–Fe/ZSM-5-25 catalysts were evaluated through consecutive recycling experiments under identical reaction conditions. After each run, the catalyst was separated from the reaction mixture by filtration, thoroughly washed with a mixed solvent of methanol and chloroform to remove residual organic species, and then dried under vacuum prior to reuse. The recovered catalyst was directly used in each cycle without further treatment. To compensate for the inevitable mass loss during the recovery process, an appropriate amount of fresh catalyst was added to maintain a constant catalyst loading. This recycling procedure was repeated for five consecutive cycles.

The chemical composition of the products was identified and quantified by gas chromatography (GC, Agilent 7890A) equipped a flame ionization detector (FID) and an HP-5MS capillary column (30 m × 0.25 mm × 0.25 μm). The oven temperature program was set as follows: an initial temperature of 50 °C held for 2 min, heated to 280 °C at a ramp rate of 5 °C min^{-1}; 280 °C for 1 min. Before GC analysis, the products were methylated with a boron trifluoride–methanol solution to derivatize unreacted fatty acids and triglycerides for accurate quantification. All

chemical components were quantified using *n*-eicosane as the internal standard. Based on the GC results, the conversion of lipids, yields of alkanes or fatty alcohols, HDO/DC selectivity ratio, and cracking degree were calculated using the following equations:

$$\text{Conversion} = (C_A - C_B)/C_A \times 100\% \quad (1)$$

where C_A represents the carbon mole of the feedstock and C_B represents the carbon molar concentration of unreacted fatty acids in the product.

$$\text{Alkane (or fatty alcohols) yield} = C_C(\text{or } C_F)/C_A \times 100\% \quad (2)$$

where C_C and C_F are the carbon moles of alkanes or fatty alcohols in the product.

$$\text{HDO/DC ratio} = (\text{C16} + \text{C18})/(\text{C15} + \text{C17}) \times 100\% \quad (3)$$

where C15, C16, C17, and C18 are the carbon moles of pentadecane, hexadecane, heptadecane, and octadecane, respectively.

$$\text{Cracking degree (light alkane yield)} = \text{C9} - 14/C_A \times 100\% \quad (4)$$

where C9–14 is the total carbon mole count of light alkanes (carbon numbers from 9 to 14), which are produced from the cracking reaction.

3. Results and discussion

3.1 Catalyst characterization

3.1.1 XRD analysis. The crystalline phases of the reduced Ni–Fe/ZSM-5-*x* catalysts with representative Si/Al ratios (15, 25, 65, and 110) were characterized by XRD, and the corresponding patterns are presented in Fig. 1. All catalysts exhibited distinct diffraction peaks at approximately 2θ = 8° and 24°, which are assigned to the characteristic reflections of the zeolite MFI framework (JCPDS PDF No. 42-0120). This confirms the successful formation of the highly crystalline ZSM-5 zeolite structure.[27] In addition, diffraction peaks located at around 44.5° and 51.8° were observed for all catalysts, which can be attributed to the metallic Ni phase (PDF 04-0850).[28] These results indicate that the Ni species were successfully reduced during the catalyst activation process. Notably, no discernible diffraction peaks ascribed to Fe species (metallic Fe, iron oxides, or iron carbides) were detected in any of the catalysts. This suggests that Fe species were highly dispersed on the ZSM-5 support below the XRD detection limit, or partially incorporated into the Ni lattice to form Ni–Fe bimetallic alloy phases, which may contribute to the synergistic interaction between Ni and Fe.

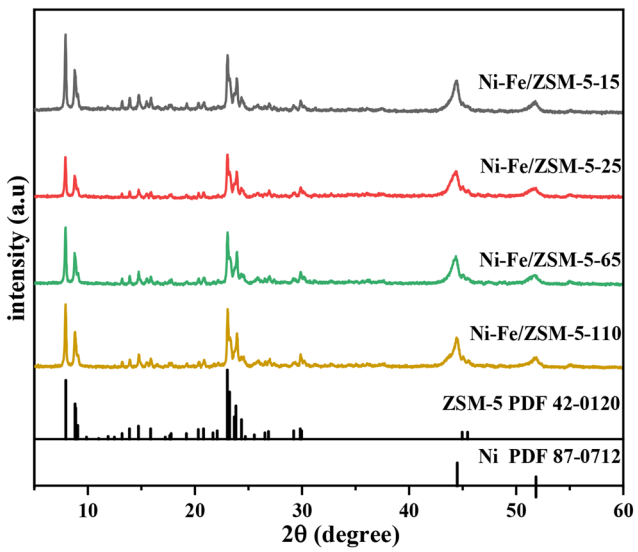

Fig. 1 XRD patterns of the reduced catalysts.

To further investigate the effect of the Si/Al ratio on the dispersion of Ni species, the average Ni crystallite size was calculated using the Scherrer equation based on the Ni(111) diffraction peak, and the results are summarized in Table 1. The Ni crystallite size increased monotonically from 8.1 nm for Ni–Fe/ZSM-5-15 to 12.9 nm for Ni–Fe/ZSM-5-110 as the Si/Al ratio increased. This trend clearly demonstrates that lower Si/Al ratios (*i.e.*, higher acidity) favor the formation of smaller and more highly dispersed Ni particles. This phenomenon can be attributed to the stronger metal–support interaction between Ni species and the more acidic ZSM-5 support, which inhibits the agglomeration of Ni nanoparticles during thermal treatment. Smaller Ni crystallites are expected to provide more exposed metallic sites for hydrogenation reactions, thereby contributing to the enhanced catalytic performance observed for catalysts with relatively low Si/Al ratios.

3.1.2 N_2 physisorption analysis. The textural properties of the Ni–Fe/ZSM-5-*x* catalysts were investigated by N_2 adsorption–desorption measurements, and the corresponding isotherms and pore size distribution curves are shown in Fig. 2. Detailed textural parameters are summarized in Table 1. According to the IUPAC classification, all samples exhibited type IV adsorption isotherms with H4 hysteresis loops, which are characteristic of hierarchical porous materials containing both micropores and mesopores.[10,29] The specific surface area increased from 252 $m^2\ g^{-1}$ for Ni–Fe/ZSM-5-15 to 285 $m^2\ g^{-1}$ for Ni–Fe/ZSM-5-25. Further increasing the Si/Al ratio resulted in a slight decrease in the surface area, reaching 271 $m^2\ g^{-1}$ and 269 $m^2\ g^{-1}$ for Ni–Fe/ZSM-5-65 and Ni–Fe/ZSM-5-110, respectively. The average pore size of Ni–Fe/ZSM-5-15 and Ni–Fe/ZSM-5-25 was approximately 1.68 nm, while catalysts with higher Si/Al ratios exhibited slightly larger pore sizes (>1.9 nm). Moreover, the pore size distribution curves verified the presence of additional mesopores around 4 nm in Ni–Fe/ZSM-5-15 and Ni–Fe/ZSM-5-25, confirming that tuning the Si/Al ratio can effectively induce the formation of hierarchical porosity in Ni–Fe/ZSM-5-*x*. The presence of hierarchical pores is favorable for lipid deoxygenation because it improves mass transfer and

Table 1 Textural properties of Ni–Fe/ZSM-5-*x* catalysts and the grain size of Ni

Catalyst	Nitrogen physisorption			Ni grain size[a] (nm)
	Surface area (m^2 g^{-1})	Total pore volume (cm^3 g^{-1})	Average pore size (nm)	
Ni–Fe/ZSM-5-15	252	0.10	1.68	8.1
Ni–Fe/ZSM-5-25	284.98	0.12	1.68	8.6
Ni–Fe/ZSM-5-65	270.85	0.12	1.91	9.2
Ni–Fe/ZSM-5-110	269.24	0.14	1.93	12.9

[a] From XRD results.

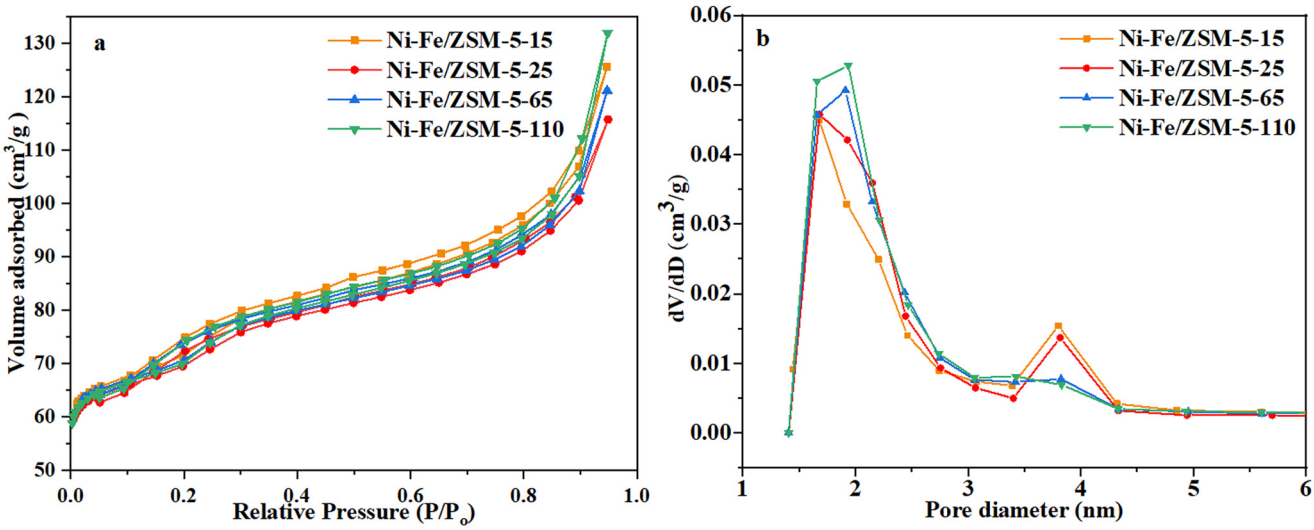

Fig. 2 N_2 adsorption/desorption isotherms (a) and the corresponding pore size distribution curves (b) of Ni–Fe/ZSM-5-*x* catalysts.

facilitates the diffusion of bulky lipid reactants and hydrocarbon products, thereby contributing to enhanced catalytic performance.

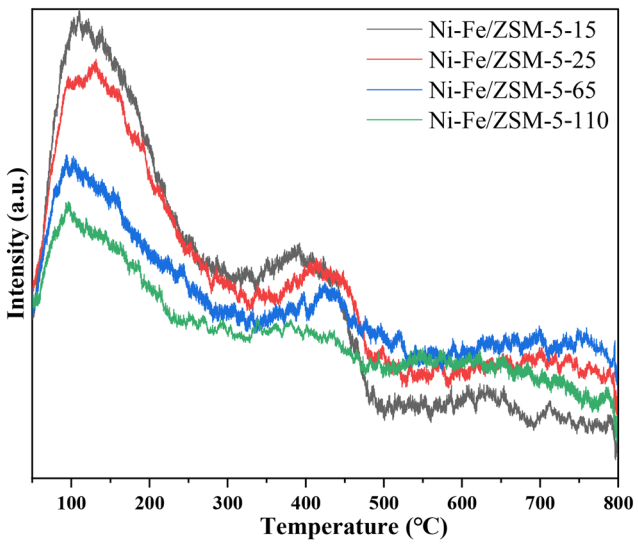

Fig. 3 NH_3-TPD curves of Ni–Fe/ZSM-5-*x*.

3.1.3 NH_3-TPD analysis. The acid properties of the Ni–Fe/ZSM-5-*x* catalysts were investigated by NH_3-TPD, and the corresponding profiles are presented in Fig. 3. All catalysts exhibited broad NH_3 desorption signals in three temperature regions of 50–300 °C, 300–500 °C, and 500–800 °C, corresponding to weak, medium, and strong acid sites, respectively. For quantitative comparison, the NH_3-TPD profiles were divided into two regions: weak acidity below 300 °C and medium-to-strong acidity above 300 °C.[30] The calculated acidity values are summarized in Table 2. Weak acid sites are mainly associated with surface silanol (Si–OH) groups or non-framework Al species, while strong acid sites originate from Brønsted acid sites formed by tetrahedrally

Table 2 Acidic properties of different Ni–Fe/ZSM-5-*x* zeolites calculated by NH_3-TPD

Sample	Acidity (mmol g^{-1})			M–S/W ratio
	Medium–strong	Weak	Total	
Ni–Fe/ZSM-5-15	0.15	0.31	0.46	0.48
Ni–Fe/ZSM-5-25	0.11	0.26	0.37	0.42
Ni–Fe/ZSM-5-65	0.09	0.16	0.25	0.56
Ni–Fe/ZSM-5-110	0.08	0.10	0.18	0.80

coordinated framework aluminum atoms.[31] As the Si/Al ratio decreased from 110 to 15, the total acidity increased significantly from 0.18 to 0.46 mmol g^{-1}, with simultaneous increases in both weak and strong acid site densities. Notably, the acidity of the catalyst exerts a decisive influence on its deoxygenation performance. In lipid hydrodeoxygenation reactions, strong acid sites serve as bifunctional active centers that promote the dehydration of intermediate fatty alcohols to form olefins, which are subsequently hydrogenated to produce alkanes over metallic Ni–Fe sites.[32,33] Therefore, appropriate strong acidity is essential for facilitating the HDO pathway and improving diesel-range alkane yields. However, excessively high acidity may induce undesired secondary cracking reactions, leading to reduced diesel selectivity, which is consistent with the performance results presented later.

3.1.4 XPS analysis. The surface chemical compositions and elemental valence states of the Ni–Fe/ZSM-5-*x* catalysts were characterized by XPS, and the corresponding spectra are shown in Fig. 4. The survey spectra clearly confirm the coexistence of Ni, Fe, Si, and Al elements on the surface of all catalysts, consistent with the expected composition of the as-prepared materials. In the high-resolution Ni 2p spectra, two distinct sets of spin–orbit splitting peaks were observed. The peaks at 852.5 eV (Ni $2p_{3/2}$) and 869.6 eV (Ni $2p_{1/2}$) are attributed to metallic Ni^0 species, while the peaks at 855.5 eV (Ni $2p_{3/2}$) and 874.4 eV (Ni $2p_{1/2}$) correspond to oxidized Ni^{2+} species, which likely arise from partial surface oxidation of metallic Ni during air exposure after passivation.[19,34] For the Fe 2p spectra, a weak peak at approximately 705.3 eV (Fe $2p_{3/2}$) is assigned to metallic Fe^0 species, and the dominant peaks at 711.8 eV (Fe $2p_{3/2}$) and 724.7 eV (Fe $2p_{1/2}$) are ascribed to Fe^{2+} species.[35,36] The low intensity of the Fe^0 signal, together with the absence of Fe-related diffraction peaks in the XRD patterns, suggests that Fe species are highly dispersed on the ZSM-5 support or partially incorporated into the Ni lattice to form bimetallic alloy phases. This structural feature may contribute to the Ni–Fe synergistic effect during

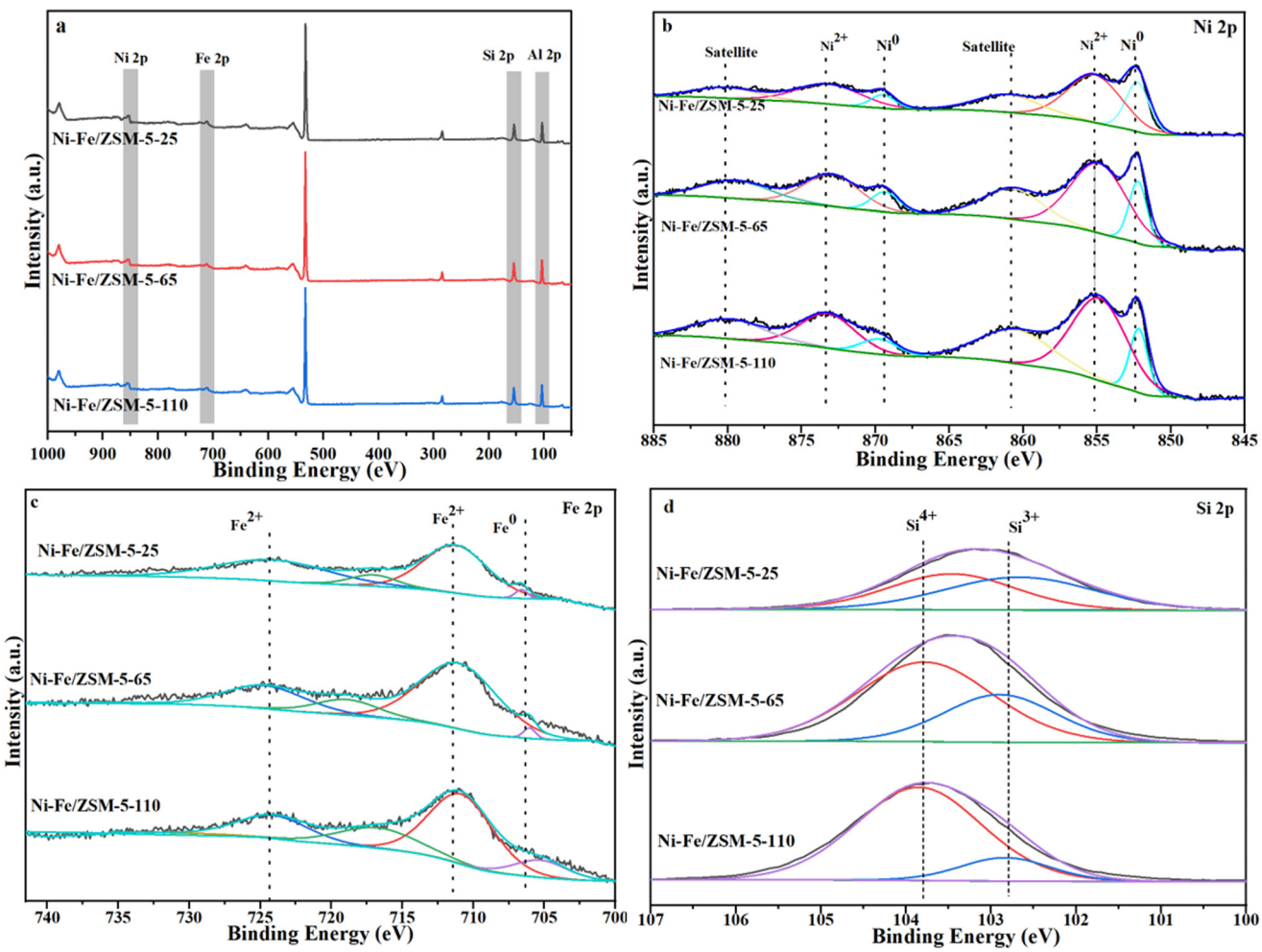

Fig. 4 XPS survey spectra (a) and high-resolution Ni 2p (b), Fe 2p (c), Si 2p (d) XPS spectra of Ni–Fe/ZSM-5-*x* catalysts.

lipid deoxygenation. In addition, the Si 2p spectra reveal two components corresponding to Si^{4+} (103.8 eV) and Si^{3+} (102.9 eV) species.[37] As the Si/Al ratio increases, the relative intensity of the Si^{4+} peak increases significantly, which is consistent with the decrease in framework aluminum content. This observation is consistent with the NH_3-TPD results, indicating that the acidity of the catalysts is closely related to the Si/Al ratio of the ZSM-5 support.

3.2 Lipid deoxygenation

3.2.1 Catalytic performance of Ni–Fe/ZSM-5-*x* catalysts. The catalytic performance of Ni–Fe/ZSM-5-*x* catalysts with different Si/Al ratios was evaluated in FA deoxygenation at 240 °C under 2.0 MPa H_2, and the results are shown in Fig. 5. The reaction products mainly consisted of four types of compounds: target diesel-range C15–C18 alkanes, octadecanol as the main intermediate, light alkanes (C8–C14) generated from secondary cracking reactions, and unconverted fatty acids. Among the hydrocarbon products, C16 and C18 alkanes are mainly produced through the HDO pathway, while C15 and C17 alkanes are generated *via* DCX/DCN pathways.[13] When the Si/Al ratio was 15, the FA conversion reached 95.5% with an alkane yield of 27.9% and a fatty alcohol yield of 67.6%. Increasing the Si/Al ratio to 25 resulted in a slight increase in alkane yield to 30.9%, accompanied by a decrease in fatty alcohol yield to 64.7%. However, further increasing the Si/Al ratio to 45 led to a sharp decline in the alkane yield to 11.3%, while the fatty alcohol yield increased to 84.9%. At a Si/Al ratio of 110, the conversion and alkane yield were 86.1% and 8.3%, respectively. Overall, Ni–Fe/ZSM-5-25 exhibited the optimal comprehensive catalytic performance, which can be attributed to the synergistic combination of its largest specific surface area (285 m^2 g^{-1}), well-dispersed Ni nanoparticles (8.6 nm), and moderate acidity (a total acid density of 0.37 mmol g^{-1}), as revealed by N_2 physisorption, XRD, and NH_3-TPD results.

Notably, the HDO/DC ratios of all Ni–Fe/ZSM-5 catalysts exceeded 7, indicating that the HDO pathway predominated over the DCX/DCN pathways. This behavior differs significantly from that observed for Ni catalysts supported on conventional supports (*e.g.* Al_2O_3 or ZrO_2), where the DCX/DCN pathways are typically dominant.[10,33,38] The preferential HDO pathway can be ascribed to the cooperation between acid sites on ZSM-5 and adjacent Ni–Fe metallic sites. Specifically, acid sites facilitate the dehydration of fatty alcohol intermediates to alkenes, while Ni–Fe metallic sites catalyze the subsequent hydrogenation of these alkenes to alkanes, thereby shifting the reaction selectivity toward HDO.[33,39] As the Si/Al ratio decreased from 110 to 15, the HDO/DC ratio increased from 7.5 to 24.4, which is consistent with the increased acid density revealed by NH_3-TPD. Importantly, the HDO-derived C16 and C18 alkanes retain the full carbon chain length of the feedstock, which is critical for maximizing hydrocarbon yield and improving process economics in industrial applications. However, excessively high acidity also promotes undesired secondary cracking reactions. As the Si/Al ratio decreased from 110 to 15, the cracking degree (light alkane yield) increased from 0.52% to 1.26%. Therefore, the moderate acidity of Ni–Fe/ZSM-5-25 achieves the optimal balance between promoting HDO activity and suppressing excessive cracking, which accounts for its superior diesel-range alkane yield.

3.2.2 Effect of reaction temperature and lipid feedstocks. Reaction temperature plays a critical role in the kinetics and product distribution of lipid deoxygenation. The catalytic performance of Ni–Fe/ZSM-5-25 in FA hydrodeoxygenation as a function of temperature is exhibited in Fig. 6a. At 220 °C, FA conversion was relatively low and a large amount of octadecanol remained in the product, suggesting that further transformation of fatty alcohol intermediates was limited at low temperature. Increasing the temperature to 240 °C

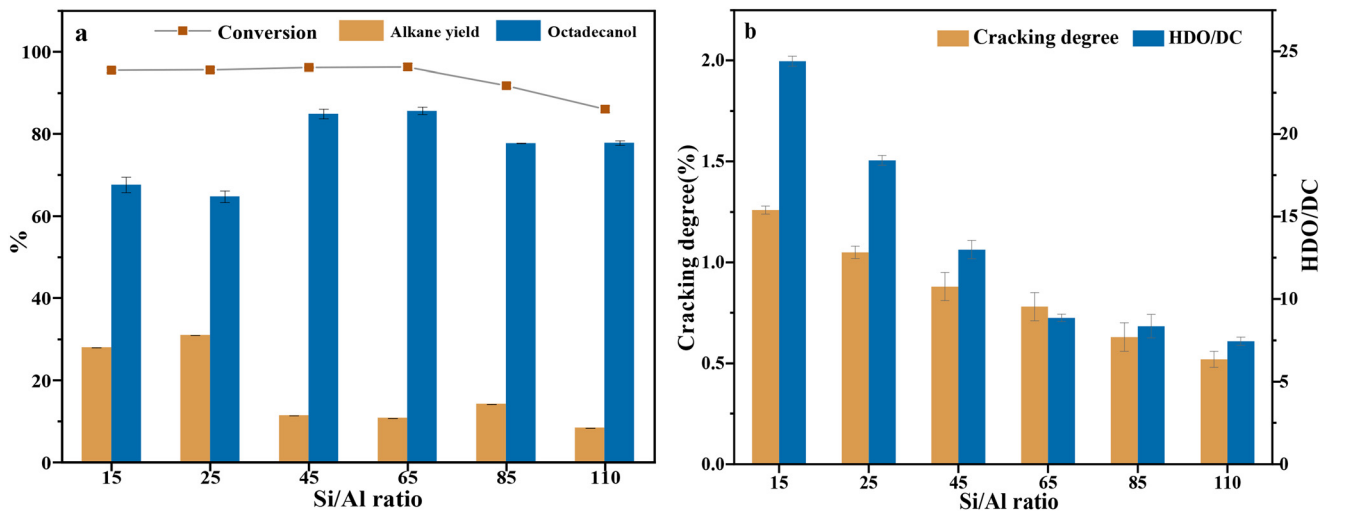

Fig. 5 Catalytic activity (a) and properties (b) of Ni–Fe/ZSM-5-*x* catalysts in FA deoxygenation.

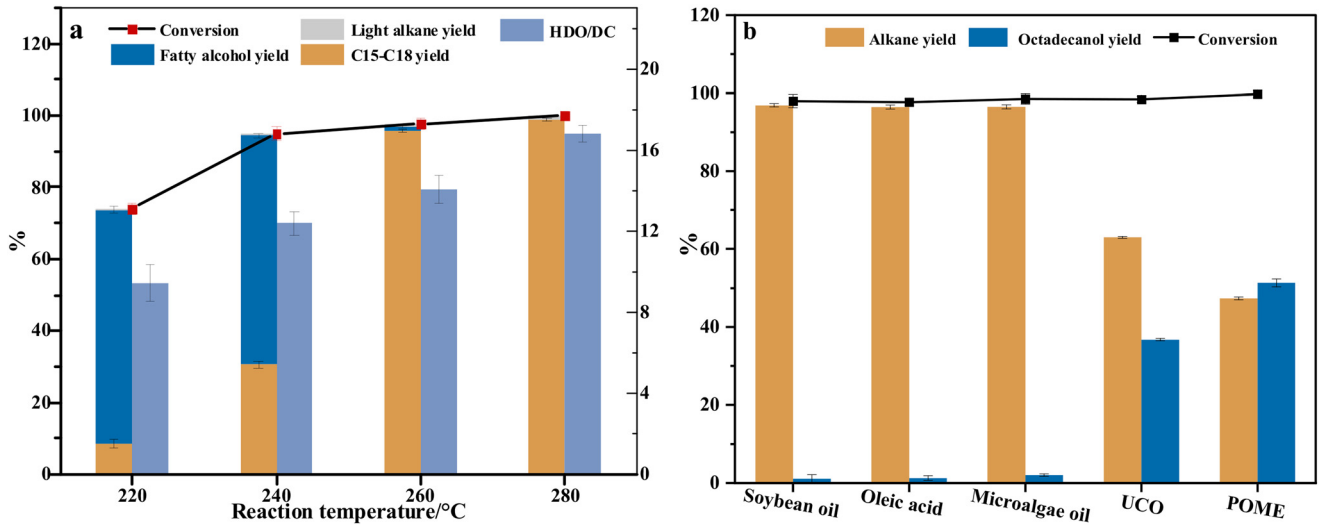

Fig. 6 Lipid deoxygenation performance over Ni–Fe/ZSM-5-25 as functions of (a) reaction temperature and (b) lipid feedstocks.

significantly improved the conversion to 95.6%, with an alkane yield of 30.9%. When the reaction temperature was further increased to 260 °C, the conversion reached 97.7%, and the alkane yield dramatically increased to 96.5%. This sharp increase in alkane yield indicates that elevated temperature facilitates the dehydration of fatty alcohol intermediates to alkenes and their subsequent hydrogenation to alkanes over Ni–Fe metallic sites. Therefore, 260 °C was identified as the optimal temperature, achieving an excellent balance between high deoxygenation activity and limited side reactions. Further increasing the temperature to 280 °C resulted in complete conversion of FA with no detectable fatty alcohol intermediates, but also led to a slight increase in the cracking degree, as evidenced by the gradual rise in the light alkane (C8–C14) yield.

The feedstock adaptability of Ni–Fe/ZSM-5-25 was further evaluated using four typical lipid feedstocks: soybean oil, microalgae oil, used cooking oil (UCO), and palm oil mill effluent (POME), with the results shown in Fig. 6b. The deoxygenation of pure soybean oil and microalgae oil exhibited performance comparable to that of FA, achieving high conversion and alkane yields. In contrast, significantly lower alkane yields were obtained when UCO and POME were used as feedstocks, with values of 63.0% and 47.3%, respectively. This performance degradation can be attributed to the presence of various impurities (*e.g.* Fe, Na, P, and Cl) in these waste oils. These impurities may block the hierarchical pore structure of the ZSM-5 support (hindering mass transfer) or poison active Ni–Fe metallic sites, thereby reducing the overall catalytic activity.

The stability and reusability of the Ni–Fe/ZSM-5-25 catalyst were evaluated in FA deoxygenation at 280 °C, and the results are presented in Fig. 7. The catalyst was consecutively reused for five cycles without any regeneration treatment. Notably, the catalytic performance remained nearly unchanged after five cycles, with FA conversion decreasing only slightly from 100% to 99.4% and alkane yield from 98.9% to 97.9%, indicating excellent catalytic stability. The high stability may be associated with the strong interaction between Ni–Fe species and the ZSM-5 support, which helps maintain the active metal dispersion and suppress structural degradation during the reaction. Furthermore, the HDO/DC ratio remained nearly constant throughout the recycling tests, suggesting that the dominant reaction pathway was well preserved during catalyst reuse. A slight increase in cracking products was observed with increasing cycle number. This phenomenon is likely related to partial surface oxidation of metallic active sites during catalyst handling and exposure to air between cycles, which may modify the acid–metal balance and promote secondary cracking reactions. Similar behavior has been reported in Ni-based systems, where oxidation or structural changes can alter product distribution without significantly affecting overall conversion.[40]

Overall, Ni–Fe/ZSM-5-25 exhibited excellent recyclability with negligible loss of activity and selectivity, demonstrating

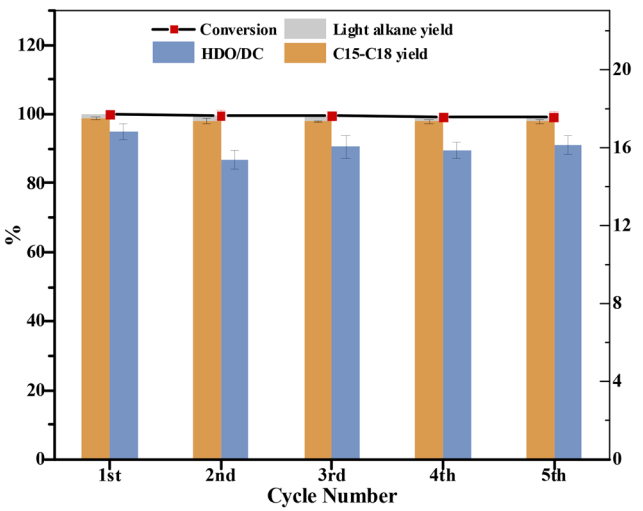

Fig. 7 Stability of the Ni–Fe/ZSM-5-25 catalyst in FA deoxygenation.

its potential for practical application in the production of green diesel *via* FA deoxygenation.

4. Conclusions

In this work, a series of bimetallic Ni–Fe catalysts supported on ZSM-5 zeolites with systematically varied Si/Al ratios of 15–110 were successfully synthesized *via* hydrothermal synthesis combined with wet impregnation, and their catalytic performance in lipid deoxygenation to diesel-range hydrocarbons was systematically investigated. The results demonstrate that the physicochemical properties of the catalysts, particularly acidity and metal–support interactions, exert a decisive influence on the catalytic activity, product selectivity and reaction pathway.

Tuning the Si/Al ratio of the ZSM-5 support precisely tailored the acid site density, metal dispersion and textural properties of the catalysts. Among all the catalysts, Ni–Fe/ZSM-5-25 exhibited the best overall performance, achieving a high FA conversion of 97.7% and an excellent diesel-range alkane yield of 96.5% under the optimized reaction conditions (260 °C and 2.0 MPa H_2). Comprehensive characterization revealed that this superior performance originated from the synergistic combination of balanced acid site distribution (a total acidity of 0.37 mmol g^{-1}), well-dispersed Ni–Fe bimetallic active species (an average Ni crystallite size of 8.6 nm) and a hierarchical pore structure. This unique structure not only facilitated the dehydration of fatty alcohol intermediates and subsequent hydrogenation to alkanes (shifting the reaction selectivity toward the carbon-conserving HDO pathway), but also effectively suppressed undesired secondary cracking reactions. The catalyst also showed excellent performance in the deoxygenation of pure vegetable oils (soybean oil and microalgae oil), demonstrating good substrate universality.

Importantly, the Ni–Fe/ZSM-5-25 catalyst exhibited excellent recyclability, maintaining high conversion and alkane yield with only negligible deactivation over multiple reaction cycles, while preserving a stable HDO/DC ratio, indicating robust structural stability and unchanged reaction pathways.

This work validates that acidity regulation of ZSM-5 supports is a highly effective strategy for designing high-performance lipid deoxygenation catalysts and provides useful insights into the development of cost-effective non-noble metal catalysts for renewable diesel production from lipid biomass.

Author contributions

Qing Li: conceptualization, methodology, formal analysis, and writing. Zihao Gao: conceptualization, methodology, formal analysis, and writing. Fumin Wang: validation, conceptualization, and review. Fei Wang: validation, methodology, formal analysis, investigation, conceptualization, writing, and review. Junfeng Feng: conceptualization and methodology. Yuwei Chen: conceptualization and methodology. Baining Lin: conceptualization, methodology, and review. Xudong Liu: methodology and formal analysis. Rukuan Liu: conceptualization, methodology, and review. Dechao Wang: validation, methodology, conceptualization, writing, and review.

Conflicts of interest

The authors declare that they have no known competing financial interests or personal relationships that could have appeared to influence the work reported in this paper.

Data availability

All data generated or analyzed during this study are included in this published article. The raw characterization data (XRD, N_2 physisorption, NH_3-TPD, and XPS) and catalytic performance data are available from the corresponding authors.

Acknowledgements

This work was supported financially by the National Natural Science Foundation of China (32401517, 32271822 and 32401523), the Major Project of the Natural Science Foundation of Universities of Jiangsu Province (22KJA480001), and the Open Foundation of the State Key Laboratory of Woody Oil Resources Utilization (No. SKLHNLKY202503). The authors would like to thank Feng Wei from Scientific Compass (https://www.shiyanjia.com) for assistance with XRD analysis.

References

1 J. Feng, L. Zhang, J. Jiang, C. Hse, T. F. Shupe and H. Pan, Directional synergistic conversion of lignocellulosic biomass with matching-solvents for added-value chemicals, *Green Chem.*, 2019, **21**(18), 4951–4957.
2 B. Barati, F. F. Zafar, L. Qian, S. Wang and A. El-Fatah Abomohra, Bioenergy characteristics of microalgae under elevated carbon dioxide, *Fuel*, 2022, **321**, 123958.
3 S. Pan, H. M. Zabed, M. Zhao, X. Qi and Y. Wei, Techno-economic and life cycle assessments for bioenergy recovery from acid-hydrolyzed residues of sugarcane bagasse in the biobased xylose production platform, *J. Cleaner Prod.*, 2023, **400**, 136718.
4 S. Lycourghiotis, E. Kordouli, K. Bourikas, C. Kordulis and A. Lycourghiotis, The role of promoters in metallic nickel catalysts used for green diesel production: A critical review, *Fuel Process. Technol.*, 2023, **244**, 107690.
5 M. Qenawy, M. Khalaf, J. Wang, J. Tian, L. Zuo and H. M. M. Mustafa, *et al.*, Performance and emission of extracted biodiesel from mixed Jatropha-Castor seeds, *Fuel*, 2024, **357**, 130060.
6 J. Suresh, N. B. Talib, N. I. W. Azelee, S. J. M. Rosid and S. Toemen, Exploring the acidic character of carbon derived from biomass waste along with potassium oxide as

bifunctional catalyst for biodiesel synthesis, *J. Environ. Chem. Eng.*, 2025, **13**(6), 119568.
7 A. M. AlSalal, F. Almomani and S. Alkanaimsh, Harnessing microalgae for a synergistic approach to CO_2 capture, wastewater treatment, and biodiesel production: A review, *J. Environ. Chem. Eng.*, 2025, **13**(5), 117465.
8 S. Hama and A. Kondo, Enzymatic biodiesel production: An overview of potential feedstocks and process development, *Bioresour. Technol.*, 2013, **135**, 386–395.
9 W. Zhong, F. Yan, J. Wang, W. Gao, G. Xu and Z. He, *et al.*, Experimental study on combustion and emission characteristics of fatty acid methyl esters and hydrogenated catalytic biodiesel/diesel blends under world harmonized steady state cycle, *Fuel*, 2023, **343**, 127887.
10 H. Zhu, F. Wang, J. Jiang, Z. Zhang, Y. Du and J. Feng, *et al.*, Ni-Fe-Al LDH derived Ni Fe nanosheet for green diesel production from lipid hydrotreatment, *Fuel Process. Technol.*, 2023, **239**, 107537.
11 R. W. Gosselink, S. A. W. Hollak, S. W. Chang, J. van Haveren, K. P. de Jong and J. H. Bitter, *et al.*, Reaction Pathways for the Deoxygenation of Vegetable Oils and Related Model Compounds, *ChemSusChem*, 2013, **6**(9), 1576–1594.
12 Y. Xie, J. Zhao, H. Wang, S. Wang, Y. Zhang and R. Li, Research progress on biodiesel production utilizing waste oils and biomass-derived catalysts, *Fuel Process. Technol.*, 2026, **281**, 108389.
13 R. Kaewmeesri, J. Nonkumwong, W. Kiatkittipong, N. Laosiripojana and K. Faungnawakij, Deoxygenations of palm oil-derived methyl esters over mono- and bimetallic NiCo catalysts, *J. Environ. Chem. Eng.*, 2021, **9**(2), 105128.
14 Y. Du, F. Wang, X. Xia, H. Zhu, Z. Zhang and C. You, *et al.*, MOF-derived Co nanoparticle on nitrogen-rich carbon for fatty acid hydrotreatment into green diesel, *Renewable Energy*, 2022, **198**, 246–253.
15 N. Chen, N. Wang, Y. Ren, H. Tominaga and E. W. Qian, Effect of surface modification with silica on the structure and activity of Pt/ZSM-22@SiO2 catalysts in hydrodeoxygenation of methyl palmitate, *J. Catal.*, 2017, **345**, 124–134.
16 J. Chen, D. Wang, F. Luo, X. Yang, X. Li and S. Li, *et al.*, Selective production of alkanes and fatty alcohol via hydrodeoxygenation of palmitic acid over red mud-supported nickel catalysts, *Fuel*, 2022, **314**, 122780.
17 J. Liu, S. Du, Z. Huang, N. Liu, Z. Shao and N. Qin, *et al.*, Enhanced Reduction of Nitrate to Ammonia at the Co-N Heteroatomic Interface in MOF-Derived Porous Carbon, *Materials*, 2025, **18**(13), 2976.
18 F. Wang, S. Yu, H. Xu, J. Feng, F. Guo and X. Jiang, *et al.*, Selective hydrogenation of oleic acid over Flower-like Ni–Fe/SiO2-ZrO2 catalyst to produce fatty alcohol: Effect of SiO2, *Fuel*, 2023, **345**, 128170.
19 F. Shi, H. Wang, Y. Chen, Y. Lu, D. Hou and C. Liu, *et al.*, Green diesel-like hydrocarbon production by H2-free catalytic deoxygenation of oleic acid via Ni/MgO-Al2O3 catalysts: Effect of the metal loading amount, *J. Environ. Chem. Eng.*, 2023, **11**(5), 110520.
20 J. Yang, Y. He, J. He, Y. Liu, H. Geng and S. Chen, *et al.*, Enhanced Catalytic Performance through In Situ Encapsulation of Ultrafine Ru Clusters within a High-Aluminum Zeolite, *ACS Catal.*, 2022, **12**(3), 1847–1856.
21 F. Yi, D. Xu, Z. Tao, C. Hu, Y. Bai and G. Zhao, *et al.*, Correlation of Brønsted acid sites and Al distribution in ZSM-5 zeolites and their effects on butenes conversion, *Fuel*, 2022, **320**, 123729.
22 S. M. Opalka and T. Zhu, Influence of the Si/Al ratio and Al distribution on the H-ZSM-5 lattice and Brønsted acid site characteristics, *Microporous Mesoporous Mater.*, 2016, **222**, 256–270.
23 D. Duan, Y. Zhang, J. Li, L. Huang, Z. Xu and Y. Zhang, *et al.*, Synthesis of nanocrystalline cellulose induced hierarchical porous ZSM-5 for catalytic conversion of low-density polyethylene, *Fuel*, 2023, **331**, 125757.
24 J. He, D. Chen, N. Li, Q. Xu, H. Li and J. He, *et al.*, Controlled fabrication of mesoporous ZSM-5 zeolite-supported PdCu alloy nanoparticles for complete oxidation of toluene, *Appl. Catal., B*, 2020, **265**, 118560.
25 T. Fu, J. Shao and Z. Li, Catalytic synergy between the low Si/Al ratio Zn/ZSM-5 and high Si/Al ratio HZSM-5 for high-performance methanol conversion to aromatics, *Appl. Catal., B*, 2021, **291**, 120098.
26 Z. Zhang, F. Wang, J. Jiang, H. Zhu, Y. Du and J. Feng, *et al.*, LDH derived Co-Al nanosheet for lipid hydrotreatment to produce green diesel, *Fuel*, 2023, **333**, 126341.
27 N. R. Demikhova, M. I. Rubtsova, G. A. Kireev, K. A. Cherednichenko, V. A. Vinokurov and A. P. Glotov, Micro-mesoporous catalysts based on ZSM-5 zeolite synthesized from natural clay nanotubes: Preparation and application in the isomerization of C-8 aromatic fraction, *Chem. Eng. J.*, 2023, **453**, 139581.
28 H. Imai, M. Abe, K. Terasaka, T. Suzuki, X. Li and T. Yokoi, Hydroconversion of methyl laurate over silica-supported Ni–Mo catalysts with different Ni sizes, *Fuel Process. Technol.*, 2018, **180**, 166–172.
29 Hartati, W. Trisunaryanti, R. R. Mukti, I. A. Kartika, P. B. D. Firda and S. D. Sumbogo, *et al.*, Highly selective hierarchical ZSM-5 from kaolin for catalytic cracking of Calophyllum inophyllum oil to biofuel, *J. Energy Inst.*, 2020, **93**(6), 2238–2246.
30 Y.-l. Wang, X.-c. Zhang, G.-g. Zhan, M.-m. Wang, W.-Q. Li and J.-p. Cao, Comparing the effects of hollow structure and mesoporous structure of ZSM-5 zeolites on catalytic performances in methanol aromatization, *Mol. Catal.*, 2023, **540**, 113044.
31 Q. Zhang, G. Chen, Y. Wang, M. Chen, G. Guo and J. Shi, *et al.*, High-Quality Single-Crystalline MFI-Type Nanozeolites: A Facile Synthetic Strategy and MTP Catalytic Studies, *Chem. Mater.*, 2018, **30**(8), 2750–2758.
32 B. Peng, C. Zhao, S. Kasakov, S. Foraita and J. A. Lercher, Manipulating catalytic pathways: deoxygenation of palmitic acid on multifunctional catalysts, *Chemistry*, 2013, **19**(15), 4732–4741.
33 F. Wang, R. Pace, Y. Ji, J. Jiang, X. Jiang and A. Krystianiak, *et al.*, Effect of Pd promotion and catalyst support on the Ni-

catalyzed deoxygenation of tristearin to fuel-like hydrocarbons, *Renewable Energy*, 2022, **195**, 1468–1479.

34 T. Li, B. Wang, P. Xu, Y. Wang, C. Wang and Q. Cui, *et al.*, Hydrodepolymerization of lignin with Ni supported on active carbon catalysts reduced at different temperatures, *Catal. Commun.*, 2024, **186**, 106826.

35 F.-P. Wu, L.-L. Qiu, Y.-P. Zhao, Z.-P. Fu, J. Xiao and J. Li, *et al.*, Hydrogen source controlled hydrodeoxygenation of phenolic compounds to cycloalkanes/cycloalkanols over NiFeAlOx catalysts, *Fuel Process. Technol.*, 2023, **252**, 107977.

36 J. Deng, X. Deng, S. Yuan, D. Ma, J. Liu and X. Xie, *et al.*, Effect of precipitating agents for the preparation of Fe-based catalysts on coal pyrolysis: Effect of Ba and Mg additives, *Fuel*, 2022, **320**, 124000.

37 I. N. Demchenko, Y. Melikhov, Y. Syryanyy, I. Zaytseva, P. Konstantynov and M. Chernyshova, Effect of argon sputtering on XPS depth-profiling results of Si/Nb/Si, *J. Electron Spectrosc. Relat. Phenom.*, 2018, **224**, 17–22.

38 K. Fani, S. Lycourghiotis, E. Kordouli, J. Zafeiropoulos, C. Kordulis and A. K. Bikogiannakis, *et al.*, Upgrading residual fatty biomass to renewable diesel over Ni based catalysts supported on natural palygorskite: the effect of promoters and reaction conditions, *Biomass Bioenergy*, 2026, **207**, 108703.

39 T. Wang, Y. Li, W. Zhang, F. Li, L. Fan and J. Fu, *et al.*, Role of Acid Centers over Ni/ZSM-5 Catalysts for Hydrodeoxygenation of Methyl Laurate to Biojet Fuels, *Ind. Eng. Chem. Res.*, 2023, **62**(40), 16513–16520.

40 K. S. Shinkevich, R. G. Kukushkin, O. A. Bulavchenko, O. O. Zaikina, M. V. Alekseeva and P. S. Ruvinskiy, *et al.*, Influence of the support on activity and stability of Ni and Ni-Mo catalysts in the hydroprocessing of fatty acids into motor fuels components, *Appl. Catal., A*, 2022, **644**, 118801.